Laser and Particle Beams (2009), *27*, 601–609.

doi:10.1017/S0263034609990322

Highly efficient, easily spectrally tunable X-ray backlighting for the study of extreme matter states

B. LOUPIAS,[1] F. PEREZ,[1] A. BENUZZI-MOUNAIX,[1] N. OZAKI,[1,2] M. RABEC,[1] L.E. GLOAHEC,[1] T.A. PIKUZ,[3] A.YA. FAENOV,[3] Y. AGLITSKIY,[4] AND M. KOENIG[1]

[1]Laboratoire Pour L'utilisation Des Lasers Intenses, Ecole Polytechnique, France
[2]Institute of Laser Engineering, Osaka University, Osaka, Japan
[3]Advanced Photon Research Center, Kansai Photon Science Institute, Japan Atomic Energy Agency, Kizugawa-city, Kyoto, Japan and Joint Institute For High Temperatures Russian Academy of Sciences, Moscow, Russia
[4]Science Applications International Corporation, Mclean, Virginia

(RECEIVED 2 May 2009; ACCEPTED 8 July 2009)

Abstract

An improved high luminosity, easily spectrally tunable backlighting scheme based on a spherically bent crystal is considered in this paper. Contrary to the traditional backlighting scheme, we used crystal far from normal incidence, and the backlighter source was inside the Rowland circle. With the presented configuration, we obtained a spatial resolution up to 8 μm in the desired direction with an X-ray backlighting energy close to 5 keV. Detailed discussions and ray-tracing calculations show that with this convenient scheme resolution down to 5 μm can be achieved. A dedicated application to high energy density physics is presented: the radiography of shock compressed matter.

Keywords: High Energy Density Physics; Laser-produced plasma; shock compressed matter; X-ray backlighting

1. INTRODUCTION

X-ray monochromatic backlighting schemes (Koch *et al.*, 1998, 1999; Cuneo *et al.*, 2005) have made numerous contributions to the current state of knowledge in inertial confinement fusion research and in other areas of laser-produced plasma study performed using laser or Z-pinch facilities. Using ns or sub-ns high-energy lasers, thermal plasma X-rays emissions have been used as backlighter to develop diagnostics. These sources have a typical spatial dimension of 50 to 400 μm and an energy range of about 1.5–6 keV. The improvement of X-ray diagnostics is today fundamental in the framework of research programs on new large facilities such as LMJ (Bordeaux) or NIF (Livermore) lasers, Z-pinch (Sandia), or an intense heavy ion beam (GSI-Darmstadt) (see for example, Cook *et al.*, 2008; Ghoranneviss *et al.*, 2008; Hoffmann *et al.*, 2000; Hora, 2007; Hora & Hoffmann, 2008; Tahir *et al.*, 2008*a*, 2008*b*; MacPhee *et al.*, 2008). Indeed, to perform quantitative measurements in the high energy density domain, backlighting schemes have to provide images of high quality (close to 10 μm spatial resolution) and over a larger energy range of 5 to 100 keV to access very dense matter. There are two main issues for construction of future backlighting schemes—optimization of backlighting source intensity for such energy range and optimization of spatial resolution of images. Intensive hard X-rays ($E > 10$ keV) can be obtained recently through relativistic electrons produced by short-pulse lasers and big efforts for optimization of K_α radiation output in such schemes are being made nowadays.

Optimization of spatial resolution of images obtained in backlighting schemes could be done by different ways. Recently, several experiments using two-dimensional (2D) point projection method have been performed to radiograph a shock compressed target, either using thermal X-rays (Miyanaga *et al.*, 1983; Marshall & Su, 1995; Stoekl *et al.*, 2008) or K_α emission (Benuzzi-Mounaix *et al.*, 2006; Ravasio *et al.*, 2008). Here, the main issues to infer density were the lack of monochromacity and the source size. Indeed, the size of the backlighter in this method has to be smaller than the expected spatial resolution (~10 μm or less). In the case of hard X-rays (K_α emission), studies of various backlighter geometries have been performed (Park *et al.*, 2006, 2008; Tommasini *et al.*, 2008; Baton *et al.*, 2008; Szabo *et al.*, 2009; King *et al.*, 2009). The results are encouraging but it remains technically difficult to

Address correspondence and reprint requests to: Anatoly Ya. Faenov, Advanced Photon Research Center, Kansai Photon Science Institute, Japan Atomic Energy Agency, Kizugawa-city, Kyoto, 619-0215, Japan. E-mail: faenov.anatoly@jaea.go.jp

produce bright X-ray point sources in order to reach the desired spatial resolution. As an alternative of X-ray point projection diagnostics, X-ray monochromatic backlighting imaging using spherically bent crystals is successfully applied nowadays (Belyaev *et al.*, 1976; Pikuz *et al.*, 1995, 1997; Aglitskiy *et al.*, 1998, 1999; Koch *et al.*, 1998, 1999; Fraenkel *et al.*, 1999; Workman *et al.*, 1999; Sanchez del Rio *et al.*, 1997; Sinars *et al.*, 2003*a*, 2003*b*; Cuneo *et al.*, 2005; Benuzzi-Mounaix *et al.*, 2006; Le Pape *et al.*, 2008). It has already been experimentally demonstrated that in the case of almost normal incidence in backlighting traditional scheme, spatial resolution around 1.6 μm could be reached within a field of view about1 mm (Aglitskiy *et al.*, 1998) and about 10 μm within a bigger field of view (4×20 mm^2) (Sinars *et al.*, 2003*a*, 2003*b*). At the same time, it is necessary to stress that for many types of high energy density physics (HEDP) investigations, it is necessary to increase the contrast of images as much as possible. Such task could be solved by using high spatially resolved monochromatic X-ray absorption imaging near K or L or M edges of used materials. It means that backlighting images should be obtained in a wide spectral range.

This point is at a serious disadvantage in the application of spherically bent crystals, because one can use them only for angles of incidence within a few degrees of normal in order to minimize the astigmatism. Such a restriction on the incidence angle, along with the fixed interplanar spacing (2D) of the crystal itself, limits the wavelengths range accessible nowadays. Moreover, it is difficult to cut and bend a spherical surface of many types of crystals with a big ratio between the crystal sizes and their radius of curvature. Therefore, the possibilities to expand the applications of this type of diagnostic in a wider energy range are very important and need to be considered.

First attempt to increase the possible energy range of spherically bent crystals backlighting scheme was done (Pikuz *et al.*, 2001; Sanchez del Rio *et al.*, 2001), where a novel scheme for backlighting imaging with some micron spatial resolution in very wide incidence angles up to 60 degrees was proposed and successfully experimentally demonstrated. Unfortunately, such a scheme allows receiving only a very low magnification 1:1, which is not convenient for HEDP experiments. Improvements of this scheme were done (Pikuz *et al.*, 2004*a*, 2004*b*), which allowed to obtain not only high quality backlighting images with different incidence angles, but also with different up to $M = 13$ magnification. Unfortunately, such scheme is also not convenient for HEDP experiments, because the investigated strongly radiated plasma should be placed in this scheme after the crystal, and radiation from plasma produces strong background on the image.

At the same time, it is necessary to remember that for many types of HEDP investigations, two very important circumstances are essential. First, the field of view usually is not so wide and could be around 1 mm in one direction and up to 10 mm in another direction. Second, usually for a shock-waves-EOS experiment, it is necessary to have a good (about 10 μm) spatial resolution only in one direction (in another direction the spatial resolution could be worse, around 20–50 μm). In this article, we propose and experimentally test improved backlighting monochromatic scheme based on spherically bent crystals, which is more convenient for HEDP physics experiments, and allowed to obtain images in a more wide energy range due to using bigger incidence angles to the crystal. In Section 2, we present the results of our configuration consisting in a 76.7° Bragg angle on a quartz crystal. In Section 3, we discuss in detail the obtained resolution by comparing them with the ray tracing code we developed. Finally in Section 4, an application to mass density measurements of shock-compressed plastic (CH) using the He_α vanadium line (close to 5 keV) is presented.

2. IMPROVED MONOCHROMATIC X-RAY BACKLIGHTING TECHNIQUE

One of the two LULI2000 beams was used to generate the X-ray source needed to perform the sample radiograph. This backlight beam was 1 ns long, smoothed with a random phase plate and focused on a 15 μm thick planar foil of vanadium with a 100 μm diameter to reach an intensity of about 10^{15} W/cm^2. The other beam was used to drive a shock on a plastic sliver. During this experiment, the X-ray radiography using a spherically bent crystal allowed us to determine the shocked plastic mass density as described in Section 4. The crystal set-up is presented in Figure 1. This quartz (11–20 orientation with 2D abut 4.9 Å) spherically

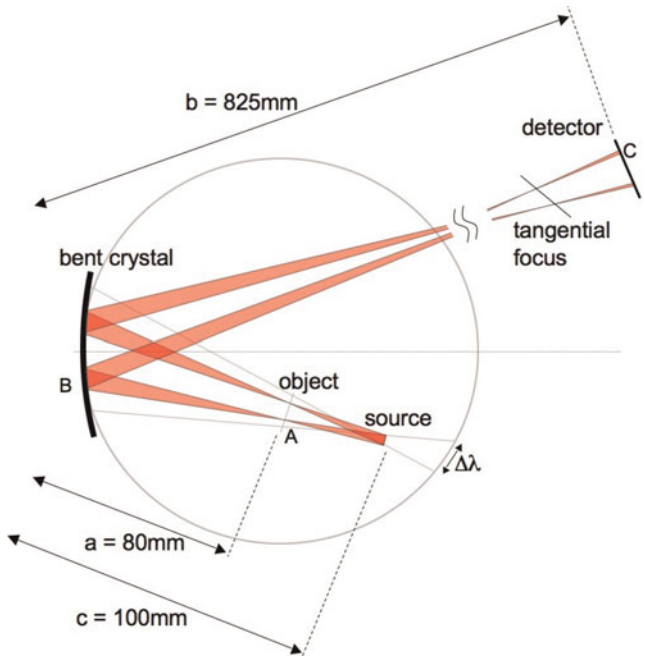

Fig. 1. (Color online) Improved backlighting scheme with a spherically bent crystal. Configuration in the tangential plane. Only formation of two points of the object on the image plane are considered in this drawing.

https://doi.org/10.1017/S0263034609990322 Published online by Cambridge University Press

bent crystal with a 15×50 mm size and a radius of $R = 150$ mm was set, according to Bragg's law, for the central wavelength $\lambda_0 \sim 2.384$ Å (Bragg angle of $\theta = 76.7^\circ$) in order to select the resonance line of Vanadium He_α at 2.382 Å and its intercombination line at 2.393 Å. It was aligned to perform an image with a magnification M ($M \sim 10$) of the object on an X-ray charge-coupled device. The large incidence angle on the crystal causes angular aberrations, which generate two focusing distances: the tangential and sagittal planes. To reduce this aberration in the tangential direction, the object was set at a distance $a = 80$ mm, the source at $c = 100$ mm from the crystal, and the detector was placed very close to the tangential focus, i.e., at a distance $b = 825$ mm. In our scheme, the X-ray source was inside the Rowland circle in order to collect more photons. Consequently, for a given spectral line, the imaged zone on the object is smaller. In such configuration, there is a compromise between intensity and field of view.

In order to measure the spatial resolution, tests have been performed using a 400 lpi grid in the object plane as shown in Figure 1. The obtained image is presented in Figure 2. We can notice, in background, the spectral intensity distribution of the source: the line on the left is the intercombination line, and the other one is the resonance line. Considering first the resonance line in Figure 2, the vertical grid wires are clearly visible in the foreground, but the horizontal ones are not so well resolved. It means that we demonstrate that a high resolution in the meridional plane, less than 10 μm, in a large field of view of about 800 μm was reached in the case of using resonance He_α line of Vanadium as a backlighter source. In the sagittal plane, the resolution was worse but still high enough with 25 μm. As the position of the detector was not optimized for obtaining images in different wavelengths of backlighter, the spatial resolution in the case of using intercombination line was not so high with about 16 μm in meridional plane, but better than for resonance line backlighting with abut 20 μm in sagittal plane. To simply sum up, we have a 2D map resolution that is the result of the image plan position in comparison with the sagittal and meridional object plan at a specific Bragg angle.

An additional test was done where the distance between object and crystal was not $a = 80$ mm like in the first experimental test, but $a = 83$ mm (Fig. 3b). The comparison of the images in Figures 3a and 3b clearly demonstrates how sensitive the spatial resolution of the obtained images depends on the position of the object. For example, in the case of object position 80 mm and He_α backlighting line, the spatial resolution is 10 μm in the meridional and 25 μm in the sagittal

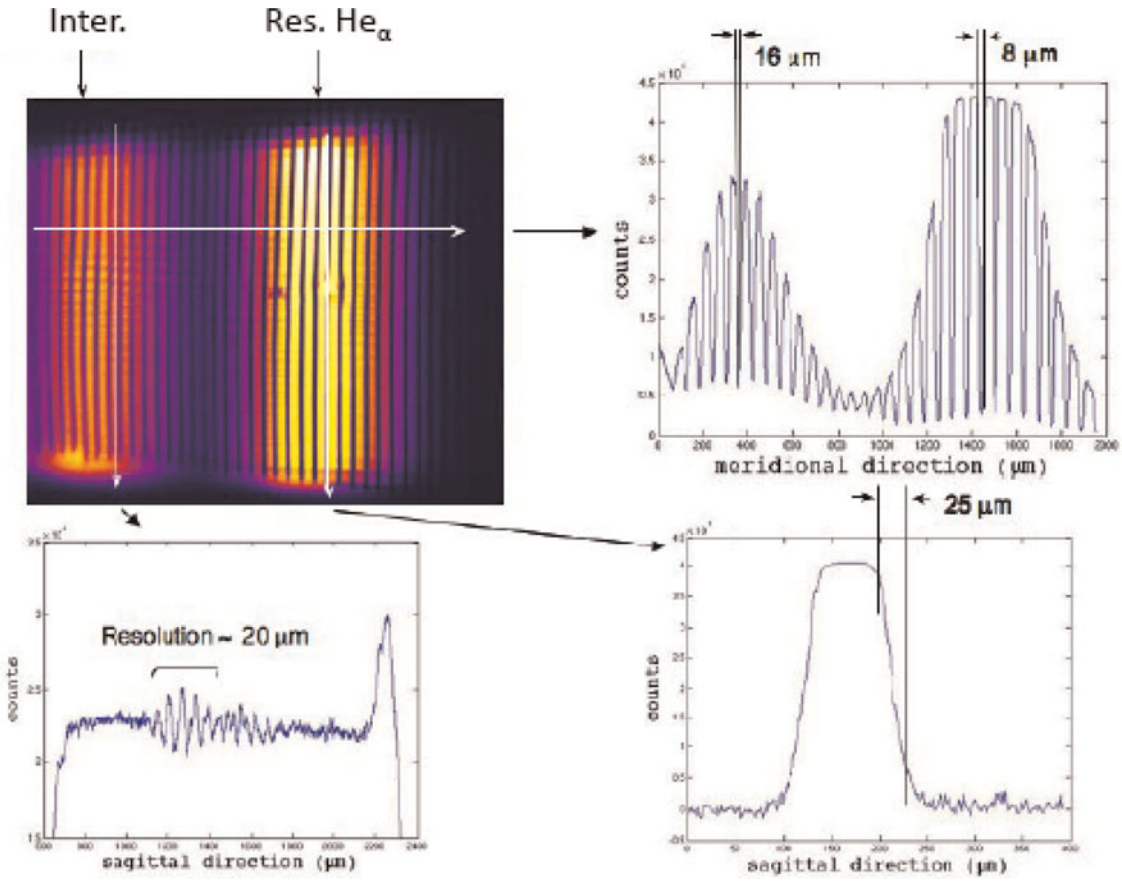

Fig. 2. (Color online) Monochromatic image of a 400 lpi gold grid and traces along the different directions of such image, obtained in the backlighting scheme of Figure 1 configuration. The distance crystal-object is 80 mm.

https://doi.org/10.1017/S0263034609990322 Published online by Cambridge University Press

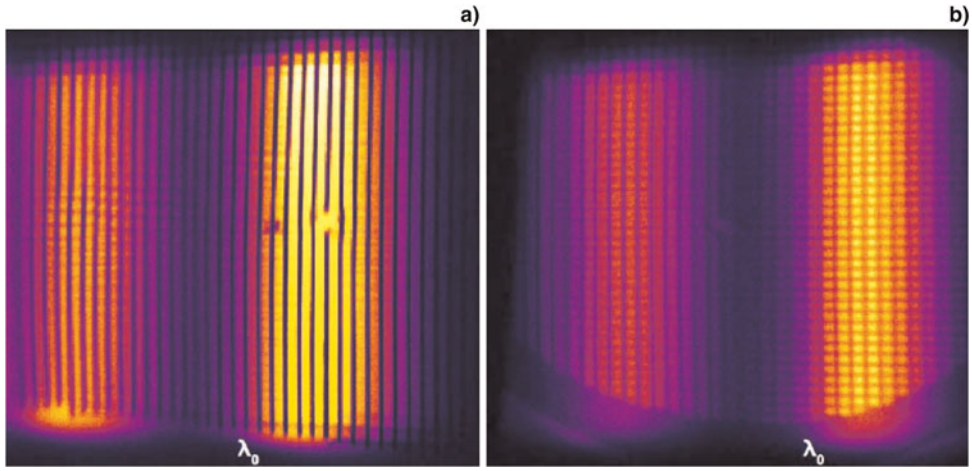

Fig. 3. (Color online) Monochromatic images of a 400 lpi gold grid. The crystal-object distance is (**a**) $a = 80$ mm and (**b**) $a = 83$ mm. The hole in the grid refers to the target chamber center.

directions, but for the case of 83 mm object position, the spatial resolution in both direction is equal and on the order of 20 μm. One may summarize, that the key point, which we demonstrated thanks to these test grid images, is the possibility to obtain high spatial resolution in a specific direction even at enough big Bragg angles instead at small Bragg angles used previously in another experiments.

3. GEOMETRICAL INTERPRETATION

To interpret the results obtained and presented in Figures 2 and 3, we developed a ray tracing code to calculate the resolution in the image plane. Let us consider one point A in the object plane which creates a spot C in the image plane (cf. Fig. 1). Its size δ must be determined in order to calculate the spatial resolution. The point A is illuminated by the source, which size is $L =$ 100 μm and which is situated at a distance of 20 mm from the object. Thus, the corresponding beam divergence is about 5×10^{-3} rad. This beam illuminates the crystal on an approximately disc shaped area B with a $\Delta = 400$ μm diameter. After the reflection on the crystal, this X-ray beam focuses at two different positions: the tangential focus f_t and the sagittal focus f_s. This implies a beam divergence that differs in both directions: $\omega_t = \Delta/f_t$ and $\omega_s = \Delta/f_s$.

In the detector plane, the diameter of the spot C, corresponding to A in the object plane, is $\delta_t = \omega_t \ |b - f_t|$ in the tangential direction and $\delta_s = \omega_s \ |b - f_s|$ in the sagittal direction (our detector is placed between the two foci). The resolutions along both directions are then $r_t = \delta_t/M_t$ and $r_s = \delta_s/M_s$, where M_t and M_s are the magnifications. The foci and magnifications can then be calculated:

$$f_t = \frac{\alpha R sin\theta}{2a - Rsin\theta}, M_t = \frac{c}{c-a}\left[\left(\frac{2}{Rsin\theta} - \frac{1}{c}\right)b - 1\right],$$

$$f_s = \frac{\alpha R}{2asin\theta - R}, M_s = \frac{c}{c-a}\left[\left(\frac{2sin\theta}{R} - \frac{1}{c}\right)b - 1\right],$$

Confusion is possible between the magnifications of the object and of the source. As we are considering the resolution in the object's plane, we gave the magnifications of the object. The same remark applies to the foci. In our scheme, this gives: $r_t < 1$ μm and $r_s \sim 33$ μm. According to the experimental picture, the sagittal resolution is reasonably explained, but the tangential resolution is not as good as 1 μm. This is mainly due to the crystal imperfections, but the resolution also depends on the position on the image. Indeed, our calculation gives the resolution only for the image center. Nevertheless, we successfully developed a ray tracing program to compute the resolution everywhere on the image.

The source spectrum has not been used to calculate the final resolution because the V He_α X-ray lines are spectrally wide enough: the corresponding area on the crystal is larger than Δ. Consequently, in our scheme, the spectral width has almost no effect on the resolution, but it controls the field of view. The spectral width has to be taken into account for a source diameter of about 500 μm.

The above discussion shows that it is possible to favor one direction against the other by moving the position either of the object or the detector. For instance, if the detector is close to the tangential focus, the resolution will be better in the tangential direction. This behavior was already observed in Section 2 with $a = 83$ mm (Fig. 3b) where the detector was half-way between the tangential and sagittal foci, giving equal resolutions in both directions. As shown on Figure 4 where only a small part of the grid is simulated, our ray-tracing program could reproduce correctly the experimental images. The sagittal and tangential resolutions correspond to the experimental data for the two different positions of the object. Indeed, the $a = 80$ mm case shows clearly that the horizontal resolution is favored, whereas the $a = 83$ mm case denotes almost equal resolutions in both directions. The program takes into account a Gaussian-shaped X-ray source in order to get a valid resolution. The spectral shape of the

https://doi.org/10.1017/S0263034609990322 Published online by Cambridge University Press

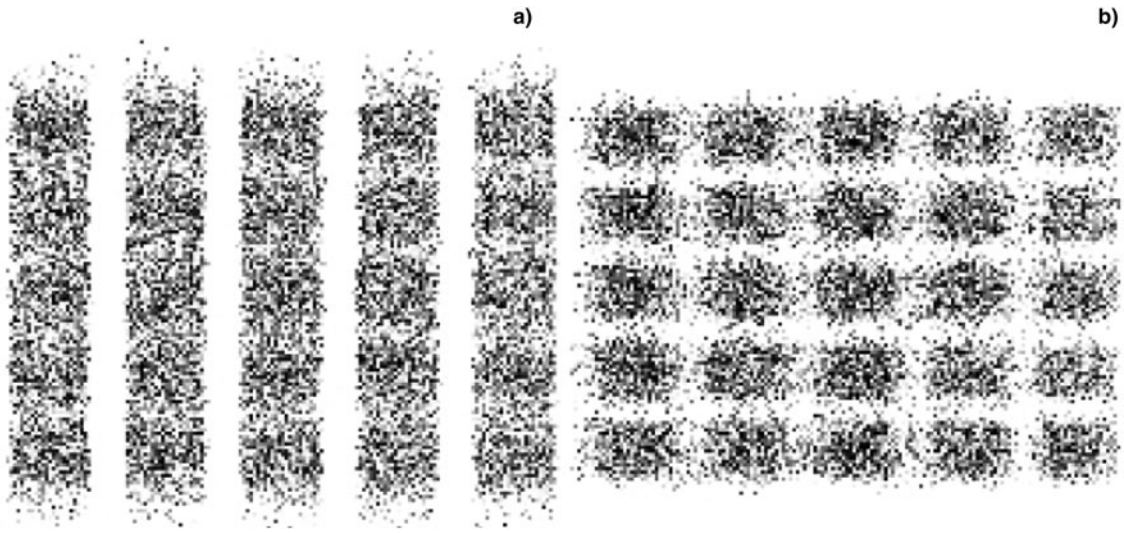

Fig. 4. Results of ray tracing modeling of image formation for a 400 lpi grid object. The crystal-object distance is (**a**) $a = 80$ mm and (**b**) $a = 83$ mm.

source is supposed to be a rectangular function of the wavelength, with a 0.006 Å width. Although the program reproduces a very similar behavior of the experimental data, the calculated resolutions are slightly better, especially a resolution better than 5 μm is predicted. This could be explained by a limited resolution due to the opacity of the grid and the shape of the wires, but another reason is probably the imperfections of the spherically bent crystal that is not taken into account in our program. A next step would be to simulate these imperfections in order to explain the limit in resolution that has also been reported in different experiments, from 2 to 10 μm depending on the crystal quality. We did implement the effect of the rocking curve, but it does not modify significantly the result. Other parameters, like a non-specula reflection, can be added, but they rely on unknown characteristics of the crystal.

At the same time, our modeling demonstrated that future experiments should be very accurately designed and alignment of crystal, object, source and detector must be very accurate. Indeed, our modeling and experimental results clearly show that spatial resolution is changed dramatically during measurements in the two rather closed configurations, $a = 80$ mm and 83 mm. Another important point, which should be considered for efficient design of such type backlighting experiments, is the role of backlighting source size for obtained spatial resolution. Indeed, Figure 5 shows the difference of the spatial resolution of image with two source sizes. One can see that, with a smaller source size ($\sim$50 μm) for our backlighting system, a significantly better resolution can be achieved. This gives a good indication on the maximum source size that should be used to optimize resolution, knowing that the crystal's imperfections cannot allow a resolution better than a few microns. Summarizing this part, we underline that the key point we want to demonstrate, thanks to this test grid images, is the possibility to obtain high spatial resolution in a specific direction even at incidence angles larger than 10° contrary to previous experiments.

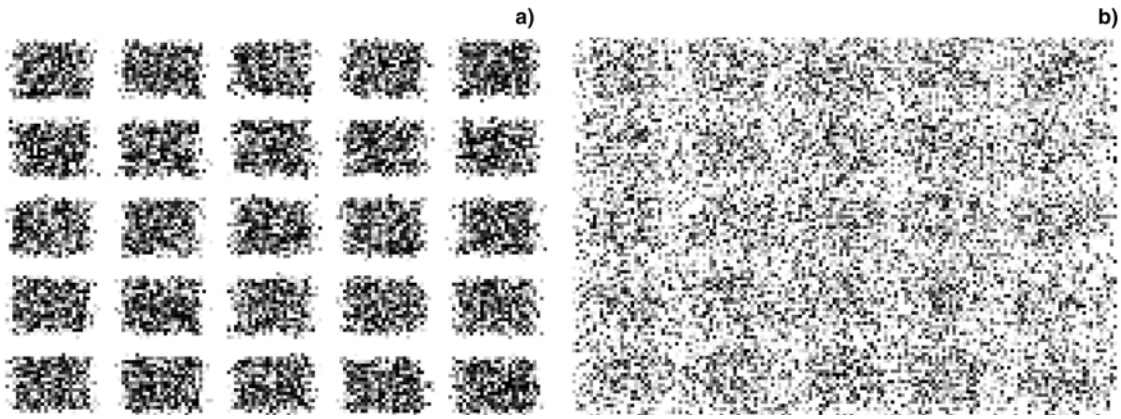

Fig. 5. The same modeling as in Figure 3b, but the source size is (**a**) $L = 50$ μm and (**b**) $L = 500$ μm.

https://doi.org/10.1017/S0263034609990322 Published online by Cambridge University Press

4. DENSITY MEASUREMENT APPLICATION AND RESULTS

One important application of X-ray sources is to radiograph and image warm dense matter with the aim to achieve a direct measurement of the mass density (Rosmej *et al.*, 2007). The backlighting scheme discussed above was used to diagnose dense plasma. In particular, radiography of shock wave propagation in solid target was performed in order to determine the mass density. Indeed, shock-wave-equations of state experiments require two parameters to be measured, like the shock and fluid velocities in order to extract the thermodynamic properties of the material. For low-Z material, X-ray radiography has been used to determine both these velocities (Cauble *et al.*, 1998; Collins *et al.*, 1998). However, the development of direct probing techniques to determine another shock parameter, such as density, would allow more precise absolute equations of state determinations and would represent a real break-through in the field. Several attempts have been made on plastic in the past (Hammel *et al.*, 1993, 1994; Ravasio *et al.*, 2008), using long-pulse laser-plasma X-ray sources. But in these experiments point projection radiography was performed. With our scheme, it is possible to reach a higher spatial resolution (10 μm) in the shock wave direction. Moreover, as the X-ray image is monochromatic, the mass density measurement of shocked plastic can be deduced with limited error bars (Benuzzi-Mounaix, 2006, 2008). These rear side diagnostics provided the shock velocity and the temperature. The general set-up of the experiment using the backlighting scheme described in this paper is presented in Figure 6a. It was performed on the LULI2000, employing one of the kJ beam to drive a shock into a plastic sliver, and another to generate the X-ray source. The laser was first focused on an ablator-pusher foil to generate a strong shock, which propagates through the plastic sliver. To cross check the density measurement from the X-ray radiography, usual shock diagnostics such as VISAR and self optical pyrometry (SOP) (Fig. 6a) were also implemented. A typical image obtained of the shock into the

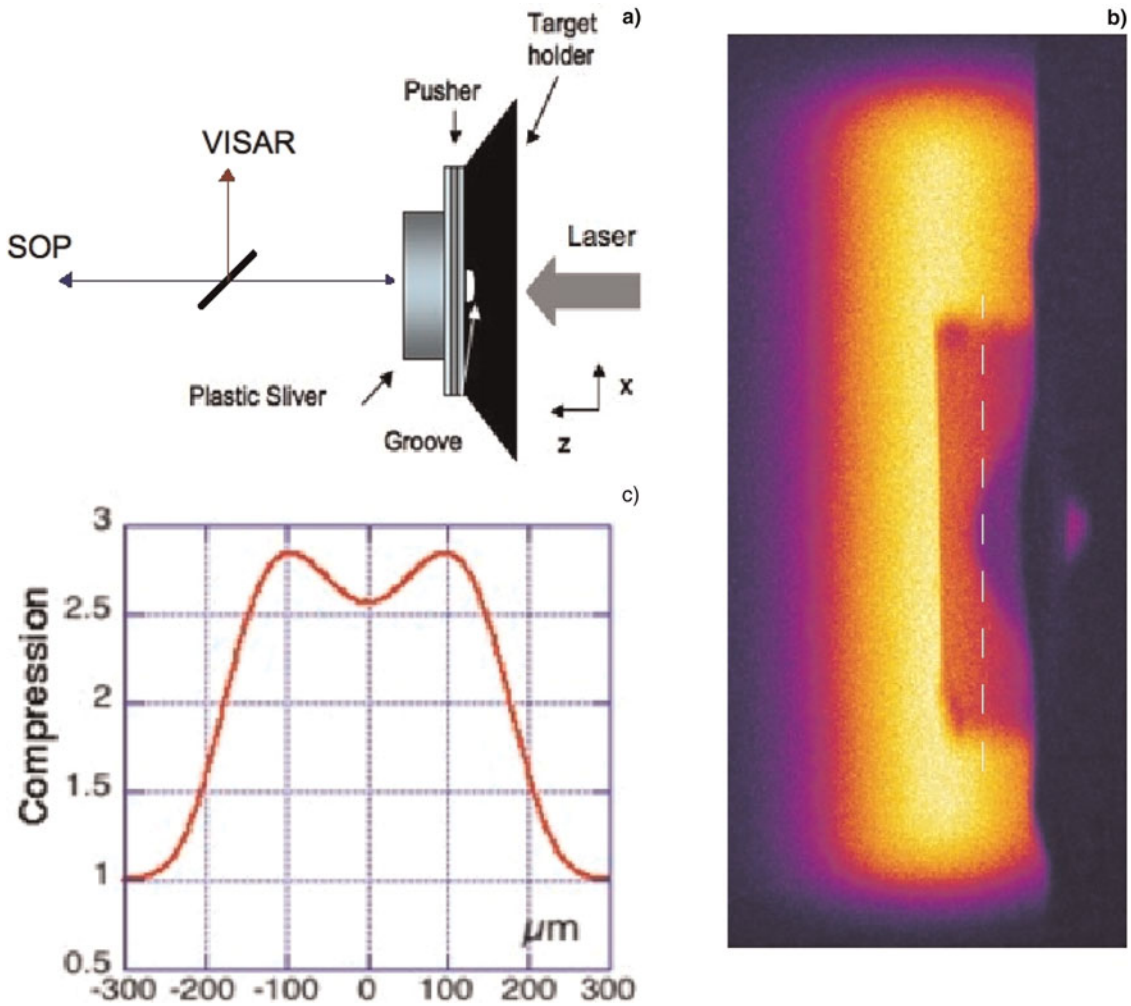

Fig. 6. (Color online) (**a**) The target is composed by a pusher, a three layer target (10 μm CH-10 μm Al – 10 μm CH) and a plastic sliver (415 μm in the radiographic direction). Self optical pyrometry and VISAR were also implemented. (**b**) X-ray shadowgraphy of the shock propagation in CH. (**c**) Compression given by Abel inversion of the shock front. The angles are larger than 10°, in contrary to previous experiments.

https://doi.org/10.1017/S0263034609990322 Published online by Cambridge University Press

Table 1. *Different spherically bent crystals and high intensity lines from plasma sources, which could be used for X-ray backlighting of plasma*

Type of crystal	2D of crystal, A	Element	Line transition	Wavelength, A	Bragg Angle
Mica 002	9.965	Mg	$K_{\alpha 1,2}$	9.89	82.8
Quartz 10–10	8.512	Al	$K_{\alpha 1,2}$	8.339	78.5
Quartz 10–11	6.666	Si	He_{α} 1s2p-1s^2	6.6479	85.8
		Al	He_{β} 1s3p-1s^2	6.6343	84.4
Mica 003	6.6473	Al	He_{β} 1s3p-1s^2	6.6343	86.4
Mica 004	4.986	Cl	$K_{\alpha 2}$	4.7307	71.6
Quartz 11–20	4.912	Cl	$K_{\alpha 2}$	4.7307	74.4
Quartz 10–12	4.564	Cl	He_{α} 1s2p-1s^2	4.4443	76.8
Quartz 20–20 2nd order 10–10	4.256	Ar	$K_{\alpha 2}$	4.19474	80.3
Mica 005	3.989	Ar	He_{α} 1s2p-1s^2	3.9489	81.9
		K	$K_{\alpha 2}$	3.7445	69.8
Quartz 11–22	3.636	K	He_{α} 1s2p-1s^2	3.5317	76.8
		Ca	$K_{\alpha 2}$	3.36166	67.6
Quartz 20–22 2nd order 10–11	3.333	Ca	He_{α} 1s2p-1s^2	3.177	72.4
Quartz 21–31	3.082	Sc	$K_{\alpha 2}$	3.0342	79.9
Mica 007	2.849	Ti	$K_{\alpha 2}$	2.75216	75.0
Quartz 20–23	2.749	Ti	$K_{\alpha 1}$	2.7485	88.9
Mica 008	2.493	V	He_{α} 1s2p-1s^2	2.3817	72.8
Quartz 22–40 2nd order 11–20	2.456	V	He_{α} 1s2p-1s^2	2.3817	75.9
		Cr	$K_{\alpha 2}$	2.29361	69.1
Quartz 31–40	2.3604	Cr	$K_{\alpha 2}$	2.29361	76.3
Quartz 40–40 4th order 10–10	2.10578	Mn	$K_{\alpha 2}$	2.10578	81.7
Quartz 22–43	2.024	Mn	He_{α} 1s2p-1s^2	2.0059	84.9
		Fe	$K_{\alpha 2}$	1.93998	73.4
Mica 010	1.995	Fe	$K_{\alpha 2}$	1.93998	76.5
Mica 011	1.813	Co	$K_{\alpha 2}$	1.79285	81.5
Mica 012	1.662	Ni	$K_{\alpha 2}$	1.6617	89
			$K_{\alpha 1}$	1.65791	86
Quartz 42–62 2nd order 21–31	1.542	Cu	$K_{\alpha 1}$	1.540562	87.5
Quartz 33–60 3rd order 11–20	1.637	Cu	$K_{\alpha 2}$	1.544398	70.6
Quartz 50–52	1.620	Ni	He_{α} 1s2p-1s^2	1.5883	78.6
		Cu	$K_{\alpha 2}$	1.544398	72.4
Mica 013	1.5343	Cu	He_{α} 1s2p-1s^2	1.47756	74.4
Quartz 53–83	1.15	Se	$K_{\alpha 2}$	1.10882	74.6
		As	He_{α} 1s2p-1s^2	1.1318	79.8
		As	Int 1s2p-1s^2	1.13862	81.9
		Au	M_1L_1	1.13525	80.8
Quartz 55–10 5th order 11–20	0.9824	Rb	$K_{\alpha 2}$	0.92969	71.1
Quartz 31–40 3d order	0.7868	Zr	$K_{\alpha 1}$	.78593	87.3

plastic sliver is shown in Figure 6b while the deduced compression across the shock front (using Abel inversion) is presented in Figure 6c. A compression (ρ/ρ_0) around 2.85 was obtained in good agreement with compression estimated using hydrodynamic simulations and data deduced from the rear side diagnostics (Benuzzi-Mounaix, 2008). To achieve a high level of accuracy in the mass density measurement, a well-known reflected spectrum range as well as a good spatial resolution is required.

5. CONCLUSION

In this paper, we demonstrated the flexibility of the X-ray radiography based on spherically bent crystals. Such a system can now be used with a larger range of angle of incidence keeping a good spatial resolution ($<10\ \mu m$). Our ray tracing calculations even suggest that improvements on the scheme used in our experiment can be achieved. In particular, limiting the source size ($\sim 50\ \mu m$) greatly enhances the resolution. In conclusion, our work opens a new era in future investigations of high energy density states. Indeed, a wider range of spherically bent crystals and backlighter configurations (a few examples in Table I) can be now employed.

ACKNOWLEDGEMENTS

This research was partially supported by the Japan Ministry of Education, Science, Sports and Culture, Grant-in-Aid for Kiban A No. 20244065, Kiban B No. 21360364, by the Russian Fund of Basic Research (Project No. 09-02-92482-MNKS_a), by RAS–CNRS Collaborative Agreement and by the RAS Presidium Program of basic researches Nos. 12 and 27.

REFERENCES

Aglitskiy, Y., Lehechka, T., Obenschain, S., Bodner, S., Pawley, C., Gerber, K., Sethian, J., Brown, C.M., Seely, J., Feldman, U. & Holland, G. (1998). High-resolution monochromatic X-ray imaging system based on spherically bent crystals. *Appl. Opt*. **37**, 5253–5361.

Aglitskiy, Y., Lehechka, T., Obenschain, S., Pawley, C., Brown, C.M. & Seely, J. (1999). X-ray crystal imagers for inertial confinement fusion experiments. *Rev. Sci. Instrum*. **70**, 530–535.

Baton, S.D., Koenig, M., Fuchs, J., Benuzzi-Mounaix, A., Guillou, P., Loupias, B., Vinci, T., Gremillet, L., Rousseaux, C., Drouin, M., Lefebvre, E., Dorchies, F., Fourment, C., Santos, J.J., Batani, D., Morace, A., Redaelli, R., Nakatsutsumi, M., Kodama, R., Nishida, A., Ozaki, N., Norimatsu, T., Aglitskiy, Y., Atzeni, S. & Schiavi, A. (2008). Inhibition of fast electron energy deposition due to preplasma filling of cone-attached targets. *Phys. Plasmas* **15**, 042706.

Belyaev, L.M., Gil'varg, A.B., Mikhailov, Yu.A., Pikuz, S.A., Sklizkov, G.V., Faenov, A.Ya. & Fedotov, S.I. (1976). X-ray photography of laser plasmas with the aid of analyzer crystals bent to form second-order surfaces. *Sov. J. Quant. Electron*. **6**, 1121–1122.

Benuzzi-Mounaix, A., Koenig, M., Ravasio, A., Vinci, T., Ozaki, N., Rabec le Gloahec, M., Loupias, B., Huser, G., Henry, E., Bouquet, S., Michaut, C., Hicks, D., MacKinnon, A., Patel, P., Park, H.S., Le Pape, S., Boehly, T., Borghesi, M., Cecchetti, M., Notley, M., Clark, R., Bandyopadhyay, S., Atzeni, S., Schiavi, A., Aglitskiy, Y., Faenov, A., Pikuz, T., Batani, D., Dezulian, R. & Tanaka, K. (2006). Laser-driven shock waves for the study of extreme matter states. *Plasma Phys. Contr. Fusion* **48**, B347–B358.

Benuzzi-Mounaix, A., Loupias, B., Koenig, M., Ravasio, A., Ozaki, N., Rabec le Gloahec, M., Vinci, T., Aglitskiy, Y., Faenov, A.Ya., Pikuz, T. & Boehly, T. (2008). Density measurement of low-*Z* shocked material from monochromatic x-ray two-dimensional images. *Phys. Rev. E* **77**, 045402.

Cauble, R., Perry, T.S., Bach, D.R., Budil, K.S., Hammel, B.A., Collins, G.W., Gold, D.M., Dunn, J., Celliers, P. & Da Silva, L.B. (1998). Absolute equation-of-state data in the 10–40 Mbar (1–4 TPa) regime. *Phys. Rev. Lett*. **80**, 1248.

Collins, G.W., Da Silva, L.B., Celliers, P., Gold, D.M., Foord, M.E., Wallace, R.G., Ng, A., Weber, S.V., Budil, K.S. & Cauble, R. (1998). Measurements of the equation of state of deuterium at the fluid insulator-metal transition. *Sci*. **281**, 1178.

Cook, R.C., Kozioziemski, B.J., Nikroo, A., Wilkens, H.L., Bhandarkar, S., Forsman, A.C., Haan, S.W., Hoppe, M.L., Huang, H., Mapoles, E., Moody, J.D., Sater, J.D., Seugling, R.M., Stephens, R.B., Takagi, M. & Xu, H.W. (2008). National Ignition Facility target design and fabrication. *Laser Part. Beams* **26**, 479–487.

Cuneo, M.E., Sinars, D.B., Bliss, D.E., Waisman, E.M., Porter, J.L., Stygar, W.A., Lebedev, S.V., Chit-tenden, J.P., Sarkisov, G.S. & Afeyan, B.B. (2005). Direct Experimental evidence for current-transfer mode operation of nested tungsten wire arrays at 16 19 MA. *Phys. Rev. Lett*. **94**, 225003.

Fraenkel, M., Zigler, A., Faenov, A.Ya. & Pikuz, T.A. (1999). Large-field high-resolution X-ray monochromatic microscope, based on spherical crystal and high-repetition-rate femtosecond laser-produced plasma. *Phys. Scripta* **59**, 246–249.

Ghoranneviss, M., Malekynia, B., Hora, H., Miley, G.H. & He, X. (2008). Inhibition factor reduces fast ignition threshold for laser fusion using nonlinear force driven block acceleration. *Laser Part. Beams* **26**, 105–111.

Hammel, B.A., Griswold, D., Landen, O.L., Perry, T.S., Remington, B.A., Miller, P.L., Peyser, T.A. & Kilkenny, J.D. (1993). X-ray radiographic measurements of radiation-driven shock and interface motion in solid density material. *Phys. Fluids B* **5**, 2259.

Hammel, B.A., Kilkenny, J.D., Munro, D., Remington, B.A., Kornblum, H.N., Perry, T.S., Phillion, D.W. & Wallace, R.J. (1994). X-ray radiographic imaging of hydrodynamic phenomena in radiation-driven materials—Shock propagation, material compression, and shear flow. *Phys. Plasmas* **1**, 1662.

Hoffmann, D.H.H., Bock, R., Faenov, A.Ya., Funk, U., Geissel, M., Neuner, U., Pikuz, T.A., Rosmej, F., Roth, M., Suss, W., Tahir, N. & Tauschwitz, A. (2000). Plasma physics with intense laser and ion beams. *Nucl. Instr. Meth. Phys. Res*. **B161**–163, 9–18.

Hora, H. & Hoffmann, D.H.H. (2008). Using petawatt laser pulses of picosecond duration for detailed diagnostics of creation and decay processes of B-mesons in the Lhc. *Laser Part. Beams* **26**, 503–505.

Hora, H. (2007). New Aspects For Fusion Energy Using Inertial Confinement. *Laser Part. Beams* **25**, 37–45.

King, J.A., Akli, K.U., Freeman, R.R., Green, G., Hatchett, S.P., Hey, D., Jamangi, P., Key, M.H., Koch, J., Lancaster, K.L., Ma, T., MacKinnon, A.J., MacPhee, A., Norreys, P.S., Patel, P.K., Phillips, T., Stephens, R.B., Theobald, W., Town, R.P.J., Van Woerkom, L., Zhang, B. & Beg, F.N. (2009). Studies on the transport of high intensity laser-generated hot electrons in cone coupled wire targets. *Phys. Plasmas* **16**, 020701.

Koch, J.A., Landen, O.L., Barbee, Jr., T.W., Celliers, P., Da Silva, L.B., Glendinning, S.G., Hammel, B.A., Kalantar, D.H., Brown, C., Seely, J., Bennett, G.R. & Hsing, W. (1998). High-energy X-ray microscopy techniques for laser–fusion plasma research at the National Ignition Facility. *Appl. Opt*. **37**, 1784–1795.

Koch, J.A., Landen, O.L., Hammel, B.A., Brown, C.M., Seely, J. & Aglitskiy, Y. (1999). Recent progress in high-energy, high-resolution X-ray imaging techniques for application to the National Ignition Facility. *Rev. Sci. Instrum*. **70**, 525–529.

Le Pape, S., Macphee, A., Hey, D., Patel, P., Mackinnon, A., Key, M., Pasley, J., Wei, M., Chen, S., Ma, T., Beg, F., Alexander, N., Stephens, R., Offerman, D., Link, A., Lynn Van-Woerkom, A. & Freeman, R. (2008). Density measurement of shock compressed foam using two-dimensional x-ray radiography. *Rev. Sci. Instr*. **79**, 106104.

MacPhee, A.G., Akli, K.U., Beg, F.N., Chen, C.D., Chen, H., Clarke, R., Hey, D.C., Freeman, R.R., Kemp, A.J., Key, M.H., King, J.A., Le Pape, S., Link, A., Ma, T.Y., Nakamura, H., Offermann, D.T., Ovchinnikov, V.M., Patel, P.K., Phillips, T.W., Stephens, R.B., Town, R., Tsui, Y.Y., Wei, M.S., Van Woerkom, L.D. & Mackinnon, A.J. (2008). Diagnostics for fast ignition science. *Rev. Sci. Instrum*. **79**, 10F302.

Marshall, F.J. & Su, O. (1995). Quantitative measurements with X-ray microscopes in laser–fusion experiments. *Rev. Sci. Instrum*. **66**, 725–727.

Miyanaga, M., Kato, Y. & Yamanaka, C. (1983). Point-source X-ray backlighting for high-density plasma diagnostics. *Appl. Phys. Lett*. **42**, 160–164.

https://doi.org/10.1017/S0263034609990322 Published online by Cambridge University Press

Park, H.-S., Chambers, D.M., Chung, H.-K., Clarke, R.J., Eagleton, R., Giraldez, E., Goldsack, T., Heathcote, R., Izumi, N., Key, M.H., King, J.A., Koch, J.A., Landen, O.L., Nikroo, A., Patel, P.K., Price, D.F., Remington, B.A., Robey, H.F., Snavely, R.A., Steinman, D.A., Stephens, R.B., Stoeckl, C., Storm, M., Tabak, M., Theobald, W., Town, R.P.J., Wickersham, J.E. & Zhang, B.B. (2006). High-energy K_α radiography using high-intensity, short-pulse lasers. *Phys. Plasmas* **13**, 6309.

Park, H-S., Maddox, B.R., Giraldez, E., Hatchett, S.P., Hudson, T., Izumi, N., Key, M.K., Le Pape, S., MacKinnon, A.J., MacPhee, A.G., Patel, P.K., Phillips, T.W., Remington, B.A., Seely, J.F., Tommasini, R., Town, R., Workman, J. & Brambrink, E. (2008). High-resolution 17–75 keV backlighters for high energy density experiments. *Phys. Plasmas* **15**, 072705.

Pikuz, S.A., Shelkovenko, T.A., Hammer, D.A., Faenov, A.Ya., Pikuz, T.A., Dyakin, A.Ya. & Romanova, V.M. (1995). High luminosity monochromatic X-ray backlighting using an incoherent plasma source to study extremely dense plasmas. *J Exper. Theor. Phys. Lett*. **61**, 638–644.

Pikuz, S.A., Shelkovenko, T.A., Romanova, V.M., Hammer, D.A., Faenov, A.Ya., Dyakin, V.M. & Pikuz, T.A. (1997). High luminosity monochromatic X-ray backlighting using an incoherent plasma source to study extremely dense plasmas. *Rev. Sci. Instr*. **68**, 740–744.

Pikuz, T.A., Faenov, A.Ya, Fraenkel, M., Zigler, A., Flora, F., Bollanti, S., Di Lazzaro, P., Letardi, T., Grilli, A., Palladino, L., Tomassetti, G., Reale, A., Reale, L., Scafati, A., Limongi, T., Bonfigli, F., Alainelli, L. & Sanchez Del Rio, M. (2001). Shadow monochromatic backlighting: Large-field high resolution X-ray shadowgraphy with improved spectral tunability. *Laser Part. Beams* **19**, 285.

Pikuz, T.A., Faenov, A.Ya., Skobelev, I.Yu., Magunov, A.I., Labate, L., Gizzi, L.A., Galimberti, M., Zigler, A., Baldacchini, G., Flora, F., Bollanti, S., Di Lazzaro, P., Murra, D., Tomassetti, G., Ritucci, A., Reale, A., Reale, L., Francucci, M., Martelluci, S. & Petrocelli, G. (2004*a*). High efficient X-ray imaging and backlighting schemes based on the spherically bent crystals. *Proceedings of SPIE*, **5196**, 362–374.

Pikuz, T.A., Faenov, A.Ya., Skobelev, I.Yu., Magunov, A.I., Labate, L., Gizzi, L.A., Galimberti, M., Zigler, A., Baldacchini, G., Flora, F., Bollanti, S., Di Lazzaro, P., Murra, D., Tomassetti, G., Ritucci, A., Reale, A., Reale, L., Francucci, M., Martelluci, S. & Petrocelli, G. (2004*b*). Easy spectrally tunable highly efficient X-ray backlighting schemes based on spherically bent crystals. *Laser and Particle Beams* **22**, 289–300.

Ravasio, A., Koenig, M., Le Pape, S., Benuzzi-Mounaix, A., Park, H.S., Cecchetti, C., Patel, P., Schiavi, A., Ozaki, N., Mackinnon, A., Loupias, B., Batani, D., Boehly, T., Borghesi, M., Dezulian, R., Henry, E., Notley, M., Bandyopadhyay, S., Clarke, R. & Vinci, T.V. (2008). Hard x-ray radiography for density measurement in shock compressed matter. *Phys. Plasmas* **15**, 060701.

Rosmej, F.B., Lee, R.W., Riley, D., Meyer-ter-Vehn, J., Krenz, A., Tschentscher, T., Tauschwitz, A., Tauschwitz, A., Lisitsa, V.S. & Faenov, A.Ya. (2007). Warm dense matter and strongly coupled plasmas created by intense heavy ion beams and XUV-free electron laser: an overview of spectroscopic methods. *J. Phys. Confer. Ser*. **72**, 012007.

Sanchez del Rio, M., Alianelli, L., Pikuz, T.A. & Faenov, A.Ya. (2001). A novel imaging X-ray microscope based on a spherical crystal. *Rev. Sci. Instrum*. **72**, 3291–3303.

Sanchez del Rio, M., Faenov, A.Ya., Dyakin, V.M., Pikuz, T.A., Pikuz, S.A., Romanova, V.M. & Shelkovenko, T.A. (1997). Ray-tracing for a monochromatic X-ray backlighting scheme, based on spherically bent crystal. *Phys. Scripta* **55**, 735.

Sinars, D.B., Bennett, G.R., Wenger, D.F., Cuneo, M.E. & Porter, J.L. (2003*a*). Evaluation of bent-crystal X-ray backlighting and microscopy techniques for the Sandia Z-machine. *Appl. Opt*. **42**, 4059–4071.

Sinars, D.B., Cuneo, M.E., Bennett, G.R., Wenger, D.F., Ruggles, L.E., Vargas, M.F., Porter, J.L., Admas, R.G., Johnson, D.W., Keller, K.L., Rambo, P.K., Rovang, D.C., Seamen, H., Simpson, W.W., Smith, I.C. & Speas, S.C. (2003*b*). Monochromatic X-ray backlighting of wire-array z-pinch plasmas using spherically bent quartz crystals. *Rev. Sci. Instrum*. **74**, 2202–2205.

Stoeckl, C., Anderson, K.S., Betti, R., Boehly, T.R., Delettrez, J.A., Frenje, J.A., Goncharov, V.N., Glebov, V.Yu., Kelly, J.H., MacKinnon, A.J., McCrory, R.L., Meyerhofer, D.D., Morse, S.F.B., Myatt, J.F., Norreys, P.A., Nilson, P.M., Petrasso, R.D., Sangster, T.S., Solodov, A.A., Stephens, R.B., Storm, M., Theobald, W., Yaakobi, B., Waxer, L.J. & Zhou, C.D. (2008). Fast-ignition target design and experimental-concept validation on OMEGA. *Plasma Phys. Contr. Fusion* **50**, 124044.

Szabo, C.I., Indelicato, P., Gumberidze, A., Holland, G.E., Seely, J.F., Hudson, L.T., Henins, A., Audebert, P., Bastiani-Ceccotti, S., Tabakhoff, E. & Brambrink, E. (2009). X-ray measurements at high-power lasers Relative conversion efficiencies of short pulse laser light into K X-ray radiation in medium to high Z elements. *Euro. Phys. J*. **169**, 243–248.

Tahir, N.A., Kim, V.V., Matvechev, A.V., Ostrik, A.V., Shutov, A.V., Lomonosov, I.V., Piriz, A.R., Cela, J.J.L. & Hoffmann, D.H.H. (2008*a*). High energy density and beam induced stress related issues in solid graphite Super-FRS fast extraction targets. *Laser Part. Beams* **26**, 273–286.

Tahir, N.A., Weick, H., Shutov, A., Kim, V., Matveichev, A., Ostrik, A., Sultanov, V., Lomonosov, I.V., Piriz, A.R., Cela, J.J.L. & Hoffmann, D.H.H. (2008*b*). Simulations of a solid graphite target for high intensity fast extracted uranium beams for the Super-FRS. *Laser Part. Beams* **26**, 411–423.

Tommasini, R., MacPhee, A., Hey, D., Ma, T., Chen, C., Izumi, N., Unites, W., MacKinnon, A., Hatchett, S.P., Remington, B.A., Park, H.C., Springer, P., Koch, J.A., Landen, O.L., Seely, J., Holland, G. & Hudson, L. (2008). Development of backlighting sources for a Compton radiography diagnostic of inertial confinement fusion targets. *Rev. Sci. Instr*. **79**, 10E901.

Workman, J., Tierney, T., Evans, S., Kyrala, G. & Benage, Jr., J. (1999). One-dimensional X-ray microscope for shock measurements in high-density aluminum plasmas. *Rev. Sci. Instrum*. **70**, 613–616.